ROYAL SOCIETY
OF CHEMISTRY

PAPER

Check for updates

Novel triphenylamine-based polyimides as promising organic cathode for lithium/sodium-ion batteries†

Lizhen Zeng, [ID] ‡[b] Yibo Chen,‡[a] Xiaotong Deng,[a] Dan Li,[a] Zhe Wang,[a] Haidong Liu,[d] Shizhu Liu,*[a] Alice A. Kasera*[c] and Ronghua Zeng [ID] *[a]

Organic carbonyl cathode materials are expected to be excellent candidates for widespread application in next-generation lithium-ion batteries (LIBs) and sodium-ion batteries (SIBs) owing to their high theoretical specific capacity, low cost, sustainability, environmental friendliness, and structural diversity. However, organic carbonyl cathode materials face some key challenges, including high solubility in organic electrolytes and low discharge platform, which hinder their practical applications. Herein, a novel poly(4-aminotriphenylamine-3,3′,4,4′-benzophenone tetamide) (PTNBI) electrode has been synthesized through the polymerization of 4-aminotriphenylamine with 3,3′,4,4′-benzophenonetetracarboxylic dianhydride (BTDA), addressing the two crucial issues of solubility and low discharge platform. As a cathode material for LIBs, the PTNBI electrode exhibits a high discharge platform of 3.5 V, and a good initial specific discharge capacity of ~135 mA h g^{-1} at 50 mA g^{-1}, whilst retaining good cycling stability after 100 cycles. The CV curves show that the redox potentials (~3.5 V/~4.0 V) correspond to the process of de-doping/doping of the PF$_6^-$ anions at the triphenylamine unit, whilst the redox potentials (~2.26 V/~2.41 V) correspond to the insertion/extraction of lithium ions at the carbonyl group of the anhydride. Meanwhile, as a cathode material for SIBs, the PTNBI electrode delivers a discharge platform of 3.0 V, and an initial specific discharge capacity of ~106 mA h g^{-1} at 50 mA g^{-1} with remarkable cycling performance. The PTNBI material incorporates a triphenylamine unit with a high discharge voltage and a carbonyl anhydride with high theoretical capacity, which effectively addresses the issues of low discharge platform and high solubility, thereby enhancing the specific capacity. This approach provides guidance for other organic electrode materials by tackling high solubility and low discharge platform challenges.

1. Introduction

Organic electrode materials have been widely applied and investigated in the field of next-generation energy storage.[1–4] Organic carbonyl-based electrode materials have been regarded as highly promising organic electrode materials for widespread application in next-generation LIBs/SIBs owing to their high theoretical specific capacities, the abundance of their raw

materials, the ability to renewably utilize them, their sustainability, structural diversity and environmental friendliness, and so on.[3,4] Based on the differences between their functional groups, carbonyl-based electrode materials can be divided into three categories: quinones, conjugated carboxylates, and imides, which are similar to anhydrides in structure.[3] However, the solubility of small-molecule organic compounds in organic electrolytes has led to serious capacity decline, so synthesizing polymers is one effective strategy to address the issue.[3,4]

As a class of conjugated carbonyl polymers, polyimides (PIs), with four carbonyl groups derived from dianhydrides, exhibit a high theoretical specific capacity (~300 mA h g^{-1}) and contain multiple aromatic rings, which provide structural stability and effectively inhibit the dissolution of the active material. Therefore, PIs have become the most attractive electrode material for LIBs/SIBs.[3,5–8] PIs can be easily synthesized through the polycondensation of aromatic dianhydrides with the electroactive centers and the diamines with the inactive linkers.[3] However, the electrochemical properties of PIs rely on the aromatic unit and have nothing to do with the diamides,[3]

[a]Guangdong Provincial International Joint Research Center for Energy Storage Materials, School of Chemistry, South China Normal University, Guangzhou, 510006, China. E-mail: zengronghua@m.scnu.edu.cn; liushizhu521@126.com

[b]Analysis and Testing Centre, South China Normal University, Guangzhou 510006, China

[c]School of Engineering, Mount Kenya University, Thika 342-01000, Kenya. E-mail: akasera@mku.ac.ke

[d]Department of Technical Physics, University of Eastern Finland, 70210 Kuopio, Finland

‡ These authors contributed equally to this work.

which reduce the actual capacity of the electrode. Thus, incorporating quinones that can participate in the reaction and can enhance the theoretical specific capacity of PIs has been pursued.[9–14] For example, Luo et al. prepared a two-dimensional (2D) microporous covalent organic framework (COF) via an in situ polymerization that integrates the polymer poly(imide-benzoquinone) (PIBN) into graphene (PIBN-G), which has been proposed to promote the redox reactions of functional groups to achieve high specific capacities and good rate performance.[12] Therefore, a high discharge capacity of 271.0 mA h g^{-1} was achieved for PIBN-G at 0.1C. Mumyatov et al. synthesized the polymer compound poly(naphthalene diimide-alt-benzoquinone) (NDI-BQ) by combining 1,4,5,8-naphthalenetetracarboxylic dianhydride (NTDA) and 2,5-diaminobenzoquinone, and the best NDI-BQ//Li cells delivered a practical capacity of 168 mA h g^{-1}.[14] Due to the introduction of an additional conjugated carbonyl group from benzoquinone, NDI-BQ, that undergoes a four-electron redox process, has a higher theoretical specific capacity of 289.5 mA h g^{-1}. It can be seen that the more conjugated carbonyl groups there are in the molecular unit, the higher the theoretical capacity of the material is. Although the theoretical capacity of PIs as cathode materials has been improved in the above studies, the average discharge voltage of the PIs was still relatively low (2.0–2.5 V).[15–17] Lei et al.[15] synthesized a submicron rectangular polyimide tube (PITs) using a hydrothermal self-templating method. At a current density of 20 mA g^{-1}, the theoretical capacity of the PITs can reach 115 mA h g^{-1}, with a discharge platform of 2.4 V. Ba et al.[16] developed a benzoquinone based polyimide by reacting a diamine monomer AQPDA containing two carbonyl groups with phthalic anhydride (PMDA) and 1,4,5,8-naphthalenetracarboxylic acid dianhydride (NTCDA) to synthesize polyimide compounds with two different aromatic chain lengths, PMAQ and NTAQ. As cathode materials for LIBs, PMAQ and NTAQ have charge discharge platform of 2.18 V and 2.25 V, respectively. At a rate of 0.1C, the average reversible capacities of PMAQ and NTAQ reach 170 mA h g^{-1} and 145 mA h g^{-1}, respectively. Wang et al.[17] synthesized a highly stable crystalline carbon nanotube-two-dimensional poly-arylimide (2D-PAI@CNT). At 0.1 A g^{-1}, the reversible capacity of 2D-PAI@CNT can reach 104.4 mA h g^{-1}, with a discharge platform of 2.4 V and a corresponding active site utilization rate of 82.9%. If the imide units are connected to structural units with high voltage,[18–21] cathode materials with higher average voltage than PIs can be obtained.

Polytriphenylamine (PTPAn) has a specific structure where the radical redox centers are stabilized and protected by a conductive polymeric backbone, and exhibits high discharge platform, good cycling stability and excellent rate capability.[18,19] Feng et al. first used PTPAn as an active material in LIBs, PTPAn exhibited a high discharge platform of 3.8 V, and a high initial discharge specific capacity of 103 mA g^{-1} at 0.5C. Meanwhile, PTPAn still displayed a 90 mA h g^{-1} capacity after 1000 cycles at 20C, thus showing long cycle stability and rate capability.[19] Chen et al. synthesized a polytriphenylamine polymer with a star-shaped structure, poly(1,3,5-(4-diphenylaminophenyl)) (PTTPAB) by chemical oxidative polymerization. PTTPAB was found to possess a high voltage platform of 3.7 V when used as a cathode material for LIBs, and provided an initial specific capacity of 86.5 mA h g^{-1} at 20 mA g^{-1}. Its rate performance (84, 82, 81, 80, 84 mA h g^{-1}) was superior to that of PTPAn (81, 73, 72, 69, 82 mA h g^{-1}), showing good rate capability and stable cycle stability performance.[20] Su et al. prepared a mesoporous conjugated polymer poly(4,4,4-tris (N,N-diphenyl-amino) triphenylamine) (PTDATA) using a chemical oxidative polymerization method. PTDATA with a nanofibrous mesoporous structure demonstrated a high voltage platform (about 3.8 V) and an initial specific capacity of 133.1 mA h g^{-1} at 20 mA g^{-1} as a cathode material for LIBs, which was equivalent to 92.8% of its theoretical capacity (143.5 mA h g^{-1}).[21] The excellent electrochemical performance of PTDATA indicated that PTPAn-based derivatives with high specific capacity and a microporous structure are excellent organic electrode materials.[21] Nonetheless, the actual specific capacity of PTPAn is generally only 90 mA h g^{-1}, and even with structural modifications, it can only reach about ~100 mA h g^{-1}, showing poor capacity performance.[22–25] In addition, the conductivity of PTPAn gradually deteriorates leading to the deactivation of the cathode material during the charge/discharge process, and thus the cycling performance will deteriorate. Therefore, it is still necessary to further optimize the structure of the PTPAn electrode material.[26,27] Chen et al. introduced an n-type naphthalimide (NTCDA) into a triphenylamine polymer chain and synthesized a triphenylamine-based polymer cathode material that can simultaneously intercalate two types of units, poly(-N,N'-bis(4-diphenylaminophenyl)-naphthalene-1,4,5,8-tetracarboxydiimide) (PTNDI). The polymer PTNDI combines the advantages of PTPAn and naphthalimide, delivering a higher theoretical specific capacity and discharge platform (2.82 V) than PTPAn alone. The initial discharge specific capacity of the PTNDI electrode delivered 140 mA h g^{-1} at 0.1C, and after 100 cycles, the specific capacity could still be maintained at 125 mA h g^{-1}.[28] Su et al. designed the synthesis of poly [2,6-bis(4-(diphenylamino)phenyl)-9,10-anthracenedione] (PBDAPA) polymers by introducing anthraquinone units with high electrochemical activity to triphenylamine. As cathode materials for LIBs, PBDAPA exhibited a high discharge platform of 3.5–4.1 V and an initial specific capacity of ~133 mA h g^{-1} at 20 mA g^{-1}, and reached 119 mA h g^{-1} after 100 cycles, whilst still maintained a capacity of 97.0 mA h g^{-1} at 200 mA g^{-1}, thus demonstrating excellent rate performance.[29]

The aforementioned works indicate that the simultaneous introduction of –C=O and N groups into polymers is beneficial for improving the discharge platform and theoretical specific capacity of electrode materials. Moreover, the conjugated structure of multiple active sites can enable polymers to have good charge transfer ability and effectively solve the solubility problem of organic materials in electrolytes. Consequently, in this work, a novel multi carbonyl polyimide derivative (PTNBI) was synthesized from BTDA and 4-aminotriphenylamine through a simple synthesis reaction and repolymerization to investigate the effect of the introduction of triphenylamine on the discharge platform, to study the effect of the polymer on solubility and investigate the insertion and extraction mechanism of PTNBI for LIBs/SIBs, thus

explaining the relationship between the structure and battery performance.

2. Experimental section

2.1. Synthesis of the 4-aminotriphenylamine-3,3′,4,4′-benzophenone tetramide (TNBI) monomer and poly(4-aminotriphenylamine-3,3′,4,4′-benzophenone tetramide) (PTNBI)

(1) Synthesis of TNBI: 1.307 g (5 mmol) of 4-aminotriphenylamine and 0.8057 g (2.5 mmol) of 3,3′,4,4′-benzophenonetetracarboxylic dianhydride (BTDA) were added to 30 mL of dimethylformamide (DMF) solvent under stirring in an N_2 atmosphere until the mixture dissolved. Then, a few drops of triethylamine were added to the solution at 120 °C for 15 min, and the mixture was refluxed at 120 °C for 3 hours under stirring. Finally, the brownish yellow product TNBI was precipitated with methanol, collected by filtration, separated using chromatography, purified with dichloromethane, and finally dried at 80 °C for 24 hours. (2) Synthesis of PTNBI: 0.675 g (4.16 mmol) of anhydrous ferric chloride ($FeCl_3$) was added to 40 mL of chloroform solvent, which was heated at 40 °C and stirred for 0.5 h under an N_2 atmosphere until the solid was completely dissolved. Then, 0.783 g (1.04 mmol) of monomeric TNBI was dissolved in 60 mL of chloroform. Finally, the two solutions were mixed together and the mixed solution was reacted at 40 °C for 24 hours. The dark brown solid PTNBI was precipitated, filtered, washed with methanol, deionized water, and an appropriate amount of dimethyl carbonate several times, purified with dichloromethane and dried at 80 °C for 24 hours.

2.2. Material characterization

The molecular structures of the TNBI and PTNBI were determined using hydrogen and carbon NMR spectroscopy (Bruker AVANCE NEO 600 Hz). The characteristic functional group vibrations of TNBI and PTNBI were measured using Fourier-transform infrared spectroscopy (SHIMADZU FT-IR 8400). The thermal stability of the TNBI and PTNBI was examined using thermogravimetric analysis (TGA) (PerkinElmer thermogravimetric analyzer). The morphological structures of TNBI and PTNBI were observed using field-emission scanning electron microscopy (ZEISS Ultra 55 with Pt-coating).

2.3. Electrochemical measurements

The working electrode was prepared from either 50 wt% TNBI or PTNBI, 40 wt% acetylene black, 10 wt% polyvinylidene fluoride (PVDF) and N-methylpyrrolidone (NMP) on Al foil. The electrodes were dried under vacuum at 80 °C for 10 h. The working electrode and the lithium/sodium foil counter electrode of the coin cell (2032) were separated by a Celgard 2300 microporous membrane and were assembled in an argon-filled glove box. The electrolyte was 1 M $LiPF_6$-EC + DMC ($V_{EC} : V_{DMC} = 1 : 1$). The loading of the active substance on a 12 mm round electrode was approximately 1.2 mg. The coin cells were assembled according to a standard procedure, and the coin cells needed to be stationary for 6 h before electrochemical testing. The charge/discharge tests were carried out in the potential range of 1.2–4.5 V versus Li/Li^+ at different constant current densities (20–200 mA g^{-1}) using a NEWARE cell test system (NEW ARE TC53). The electrolyte employed in the SIB was 1 M $NaClO_4$-EC + DMC ($V_{EC} : V_{DMC} = 1 : 1$). Cyclic voltammogram (CV) curves were conducted on a CHI660D electrochemical workstation in a potential range of 1.2–4.5 V at the scanning rate of 0.1 mV s^{-1}. Electrochemical impedance measurements were carried on a CHI660D electrochemical workstation (frequency range: 10^{-2} to 10^5 Hz, voltage amplitude: 5 mV). In addition, the theoretical specific capacity and coulombic efficiency (CE) for TNBI and PTNBI can be obtained according to the following equation:

$$C_t \text{ (mA h g}^{-1}) = n \times F/M_w \tag{1}$$

C_t, n, F, and M_w are the theoretical specific capacity, active electron number, faradaic constant and molecular weight, respectively.

Coulombic efficiency (CE) = discharge specific capacity/charge specific capacity × 100%. (2)

3. Results and discussion

3.1. Structural characterization

The synthetic route used to obtain TNBI and PTNBI is shown in Fig. 1 and the details are provided in the Experimental section. The chemical structure, functional groups, thermal stability and morphology of TNBI and PTNBI were characterized using NMR, FTIR, SEM, and TGA, respectively. The ^1H NMR spectrum of TNBI is displayed in Fig. S1(a).† It can be seen that the peak positioned between 8.0–8.5 ppm is attributed to the H on the imide ring and the peak positioned between 6.7–7.5 ppm is ascribed to the H atoms of triphenylamine. This differs from the ^1H NMR spectrum of BTDA and 4-aminotriphenylamine (Fig. S2†), confirming that BTDA and 4-aminotriphenylamine react to form TNBI. As can be seen from the ^{13}C NMR spectrum of TNBI (Fig. S1(b)†), the carbon of the imide ring is located between 160–200 ppm, and the carbon of the triphenylamine is located between 120–150 ppm, which also confirmed the successful synthesis of TNBI.

Fig. 2a is FTIR spectra of TNBI and PTNBI. As shown in Fig. 2a, the structures of TNBI and PTNBI are consistent, the absorption peak located at 3050 cm^{-1} corresponds to the stretching vibration of C–H on the benzene ring, the absorption peak of 1499 cm^{-1} corresponds to the stretching vibration of the C=C bond on the benzene ring, and the absorption peaks of 1720 cm^{-1} and 1672 cm^{-1} are assigned to the stretching vibration peaks of C=O in the hexagonal imide ring, indicating the presence of the conformational structure of the imide ring.[30]
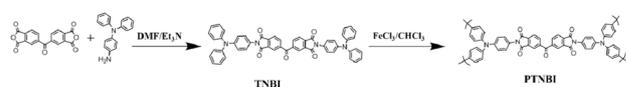

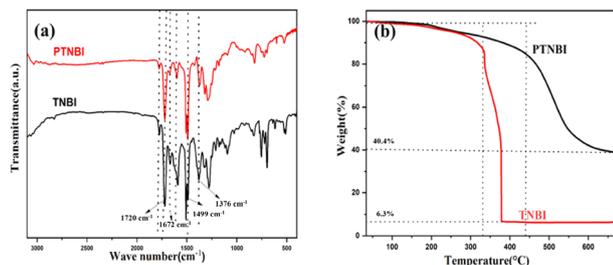**Fig. 1** Synthetic route used to obtain monomer TNBI and polymer PTNBI.

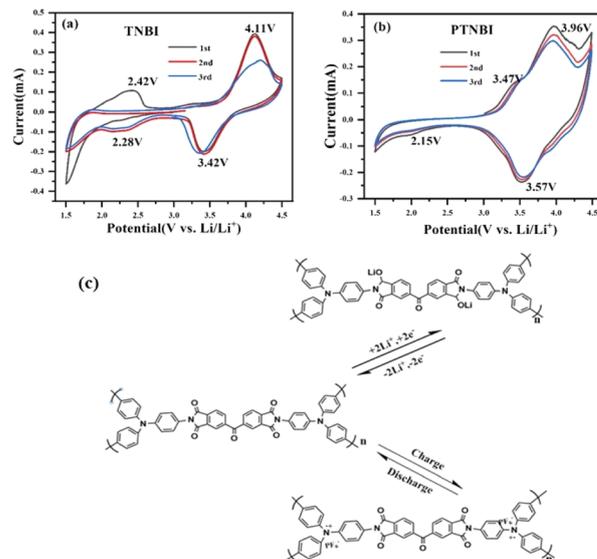**Fig. 2** FT-IR spectra (a) and TGA curves (b) of TNBI and PTNBI.

Fig. 3 CV curves of (a) TNBI and (b) PTNBI in LIBs, scan rate: 0.1 mV s^{-1}. Electrochemical reaction mechanism of the polymer PTNBI in LIBs (c).

The absorption peak at 1376 cm^{-1} is attributed to the stretching vibration peak of C–N, suggesting that both TNBI and PTNBI formed the characteristic imide ring. Compared with TNBI, the absorption intensity of PTNBI at 745 cm^{-1} and 695 cm^{-1}, belonging to the out-of-plane bending vibration of C–H in the monosubstituted benzene ring, is weakened. Thus, it is further demonstrated that TNBI and PTNBI have been successfully synthesized. Fig. 2b displays the TGA curves of TNBI and PTNBI. TNBI begins to decompose at 200 °C, rapidly loses weight at 335 °C with a residual weight of 6.3% at 800 °C. Meanwhile, PTBNI rapidly loses weight at 448 °C with a residual weight of 40.4%. It can be seen that polymerization to create PTNBI can enhance the thermal stability and safety of TNBI. Fig. S3† shows the morphology of TNBI and PTNBI. As displayed in Fig. S3a and b,† TNBI exhibits a large irregular block structure with an average diameter of 5–10 μm and a relatively smooth surface. However, the PTNBI appears as sphere-like agglomerates with an average diameter of 0.5–1 μm and wrinkled protrusions on the surface of the spherical structure (Fig. S3c and d†). Fig. S4† shows the images of the TNBI and PTNBI electrodes dissolved in the electrolyte (EC : DMC = 1 : 1) after different soaking durations. The TNBI electrode quickly changes colour in the electrolyte before and after seven days of soaking. While, the polymer PTNBI electrode is nearly unchanged in the electrolyte, which indicates that PTNBI has excellent insolubility characteristics in electrolytes.

3.2. The mechanism of insertion and extraction of lithium ions in TNBI and PTNBI

CV curves were used to explore the lithium ion insertion and extraction mechanism in the TNBI and PTNBI electrodes. As shown in Fig. 3a, TNBI has two different pairs of reversible redox peaks at 2.28 V/2.42 V and 3.42 V/4.11 V, respectively. The redox peaks located at ∼2.28 V/∼2.42 V are attributed to the redox reaction of the carbonyl group in the imide units, corresponding to the process of lithium ion insertion/extraction at the carbonyl groups at the ends of the imide ring (Fig. 3c).[28,31] The redox peaks at high potentials of ∼3.42 V/∼4.11 V are associated with the doping/de-doping process of PF$_6^-$ at the nitrogen cations in the triphenylamine unit (Fig. 3c).[28,31,32] At a high potential of ∼4.1 V, the nitrogen group loses electrons while being accompanied by the development of PF$_6^-$ at the nitrogen group, and the reduction occurs at ∼3.42 V, indicating the process of doping PF$_6^-$ was successful. For PTNBI (Fig. 3b), there is a reversible redox peak at

∼3.57 V/∼3.96 V, which also corresponds to the doping/de-doping process of PF$_6^-$ at the nitrogen cation of the triphenylamine unit. Additionally, a weak reduction peak for the imine ring carbonyl group (C=O) appears at ∼2.15 V, corresponding to the intercalation of Li$^+$ at the carbonyl group. It can be seen in Fig. 3a and b that both of PTNBI and TNBI have similar redox peaks, and the coincidence of the CV curves is high, suggesting that they have good cycle reversibility. It is worth noting that PTNBI exhibits an oxidation peak with 3.47 V, which is attributed to the n-doping of the carbonyl groups on the imide rings. Due to the charge trapping effect (CT effect), n-doped polymers undergo charge capture at low potentials.[33,34] Therefore, the oxidation peak at a high potential of ∼3.5 V can be ascribed to charge elimination under the CT effect.

3.3. Charge and discharge performance of TNBI and PTNBI

The charge and discharge performance of TNBI and PTNBI were investigated over a voltage range of 1.5 V to 4.5 V. As displayed in Fig. 4a and b, the TNBI electrode exhibits an initial discharge capacity of ∼78 mA h g^{-1} at 25 mA g^{-1}, which is about 34% of the theoretical capacity (232 mA h g^{-1}, eqn (1)). The discharge specific capacity is reduced to ∼40 mA h g^{-1} after 50 cycles. It is worth noting that there are two discharge platforms at ∼2.3 V and ∼3.4 V in the first discharge cycle of TNBI, which correspond to the process of embedding Li$^+$ on the carbonyl group and the process of de-doping of PF$_6^-$ from the triphenylamine nitrogen group, respectively. In addition, two charge platforms are observed at ∼2.4 V and ∼4.1 V, corresponding to the de-lithiation of the carbonyl group and the doping process of PF$_6^-$ at the nitrogen group. In the second charging process, there are no obvious charge platforms at ∼2.5 V and below, and only the plateaus of the de-doping of PF$_6^-$ from the triphenylamine nitrogen group were obviously observed at ∼4.1 V. Meanwhile, the PTNBI electrode exhibits an initial discharge capacity of ∼138 mA h g^{-1} at
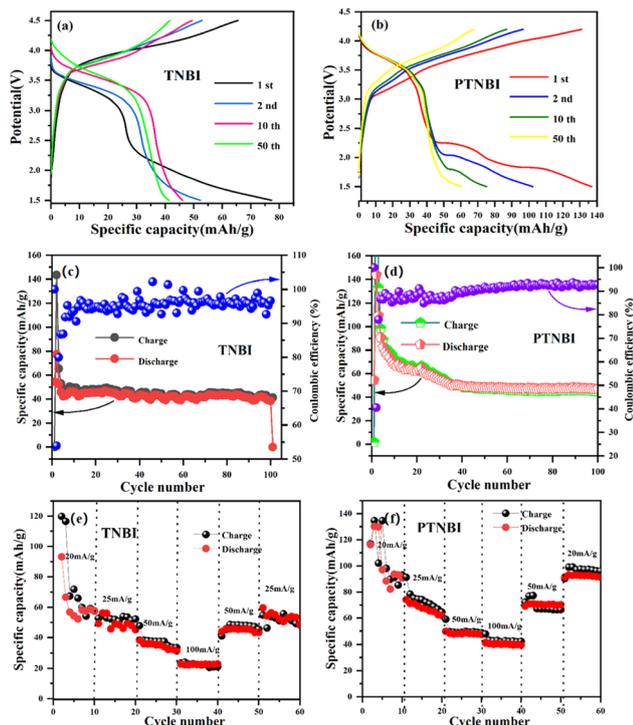
Fig. 4 Charge/discharge curves of TNBI (a) and PTNBI (b) in LIBs, current density: 25 mA g^{-1}. Cycling performance of TNBI (c) and PTNBI (d) in LIBs, current density: 50 mA g^{-1}. Rate capability of TNBI (e) and PTNBI (f) in LIBs.

25 mA g^{-1}, which is about 60% of the theoretical value. After 50 cycles, the discharge specific capacity is ~60 mA h g^{-1}. It can be seen that the cycle performance of the PTNBI electrode is better than that of TNBI electrode. Additionally, it can be seen that the two discharge and charge platforms during the first and second cycle are also obviously observed at ~2.3 V/~3.4 V and ~2.4 V/~3.9 V, respectively. As the number of cycles increases, the charge/discharge platforms below ~2.5 V gradually disappear. Only the doping and de-doping process of PF$_6^-$ in the triphenylamine nitrogen group in the range of 3.0–4.3 V are observed. This may be because triphenylamine is a strong electron donor which limits the n-doping to a certain extent.[35]

Long-term cycling stability tests were conducted on the TNBI and PTNBI electrodes in a voltage range of 1.5–4.5 V. As shown in Fig. 4c, the TNBI electrode has an initial discharge-specific capacity of ~80 mA h g^{-1} at 50 mA g^{-1} with a capacity retention rate of only 38% after 100 cycles, whilst the cycling stability was poor and the coulombic efficiency was 70% (eqn (2)). As displayed in Fig. 4d, the PTNBI electrode exhibits a discharge specific capacity of ~135 mA h g^{-1} at 50 mA g^{-1} with a capacity retention rate of 43% after 100 cycles and a coulombic efficiency of over 90%. It can be seen that TNBI has a smaller molecular weight and is easily soluble in aprotic electrolytes, resulting in rapid capacity decay and lower coulombic efficiency. However, the higher molecular weight of PTNBI effectively inhibits its dissolution in the electrolyte, resulting in slower capacity decay and maintaining the structural stability during the lithium-ion deintercalation and intercalation process.[34] Therefore, PTNBI has better long-term

cycling stability and higher capacity than TNBI. The rate performance of the TNBI and PTNBI electrodes was also tested at different current densities. As shown in Fig. 4e and f, at current densities of 20, 25, 50, and 100 mA g^{-1}, the TNBI electrode delivers average discharge capacities of ~80 mA h g^{-1}, ~50 mA h g^{-1}, ~40 mA h g^{-1}, and ~20 mA h g^{-1}, respectively. While the PTNBI electrode delivers average discharge capacities of ~100 mA h g^{-1}, ~80 mA h g^{-1}, ~50 mA h g^{-1}, and ~40 mA h g^{-1} at the same current density, respectively. When the current density is restored to 20 mA g^{-1}, the discharge capacity of PTNBI can recover to around ~100 mA h g^{-1}. It can be seen that the rate performance results are consistent with the results of the cycling performance, indicating that PTNBI has better rate performance than TNBI. The above charge and discharge results show that the overall charge and discharge performance of PTNBI is superior to that of TNBI.

To further explain the good electrochemical performance of PTNBI in comparison to that of TNBI, electrochemical impedance spectroscopy (EIS) was carried out to investigate the charge transfer resistance of PTNBI and TNBI. The semicircle reflects the charge transfer resistance (R_{ct}). Fig. S5† shows that the diameter of the semicircle for PTNBI is smaller than that of TNBI before cycling and after 100 cycles, which indicates that PTNBI has a lower R_{ct} during the charge and discharge process. This finding suggests that PTNBI has faster reaction kinetics and that the structure of PTNBI is not destroyed, thereby demonstrating the superior electrochemical performance of PTNBI. The surface morphologies of TNBI and PTNBI before and after 100 cycles were tested to further explore the structural stability of TNBI and PTNBI. Fig. S6a† shows that the morphology of TNBI before cycling is a sheet-like structure. After 100 cycles (Fig. S6b†), the morphology of TNBI is not apparent, indicating that a large part of the TNBI has been dissolved in the electrolyte, confirming the poor cycling performance of TNBI. As shown in Fig. S6c,† PTNBI has a sphere-like structure before cycling. After 100 cycles (Fig. S6d†), the sphere-like structure could still be observed for the PTNBI electrode. It can be seen that no structural change or damage was observed. These results indicate that PTNBI is more stable than TNBI and has a lower solubility in the electrolyte, so it has better cycling stability. To compare the performance of PTNBI with other polymers, Table S1† presents a comparison of the charge and discharge performance of the PTNBI electrode with other organic cathode materials reported in the literature. As can be seen from the Table S1,† the PTNBI material has the highest redox potential (3.5 V), and the theoretical specific capacity and actual specific capacity are better than the literature reports given in the table.[7,14–16] From the structure of the polymer, it can be observed that the high potential structure of triphenylamine contributes to a higher redox potential in the polymer material. Meanwhile, the greater number of active sites (five –C=O groups in PTNBI) provide the electrode material with a higher theoretical specific capacity.

3.4. Sodium-ion storage mechanism and charge and discharge performance of PTNBI

To explore the mechanism of insertion and extraction of Na$^+$ in PTNBI, the CV test was performed on PTNBI over a voltage range

Paper

of 1.5–4.5 V and a scan rate of 0.1 mV s^{-1} (Fig. 5). There is a reversible redox peak at ~3.65 V/~3.58 V in the first cycle (Fig. 5a), which is attributed to the doping/de-doping process of ClO_4^- at the nitrogen group of the triphenylamine unit (Fig. 5b). Additionally, a pair of obvious redox peaks appear at ~2.38 V/~2.18 V, corresponding to the intercalation/de-intercalation process of Na$^+$ at the carbonyl groups (C=O) in the anhydride. Compared with the redox peaks of PTNBI in LIBs, the peak is more obvious. It is worth noting that a separate oxidation peak appears at around ~3.5 V, which disappears after the second cycle. The oxidation peaks at high potentials may be due to the CT effects during cycling process, leading to a higher oxidation potential and greater peak current when the charge is released during n-doping of the carbonyl functional group at high potential.[33,34] It can be seen from the CV curves that the coincidence of the curve peaks is good, indicating that PTNBI exhibits excellent cycling stability in SIBs.

Fig. 6a shows the charge–discharge curves of PTNBI at 20 mA g^{-1} for the first 10 cycles. As displayed in Fig. 6a, the PTNBI has an initial charge–discharge capacity of ~250/~90 mA h g^{-1} with a cycle coulombic efficiency of 37% for the first cycle. After 10 cycles, the charge–discharge specific capacity is ~70/~60 mA h g^{-1}. The PTNBI electrode exhibits two discharge platforms in the charge–discharge curves, which is consistent with the redox peak in the CV curves. Then, the low-potential plateaus gradually disappear, the irreversible loss of capacity of PTNBI is observed in the first cycle, which may be due to the formation of a CEI film, leading to capacity decay.[34] To further study the cycling performance and rate capability of PTNBI as a cathode for SIBs, PTNBI was subjected to cycling performance tests (Fig. 6b) and rate performance tests (Fig. 6c). As displayed in Fig. 6b, the initial discharge capacity of PTNBI is ~106 mA h g^{-1} and the capacity decays to ~47 mA h g^{-1} after 50 cycles. Fig. 6c shows the rate performance of PTNBI at different current densities. When the current densities are 20 mA g^{-1}, 50 mA g^{-1}, 100 mA g^{-1} and 200 mA g^{-1}, PTNBI exhibits average specific capacities of ~100 mA h g^{-1}, ~62 mA h g^{-1}, ~41 mA h g^{-1}, and ~30 mA h g^{-1}, respectively. When the current density is returned to 20 mA g^{-1}, the discharge specific capacity recovers to ~52 mA g^{-1}. The charge and discharge performance tests show that the PTNBI electrode has good cycling and rate performance in SIBs.

To study the structural composition, structural stability and morphology changes of the electrode materials during cycling of the SIBs, FTIR, SEM and EIS were conducted on the PTNBI
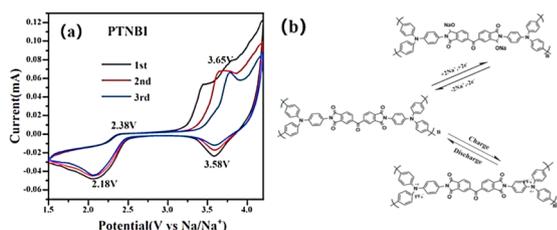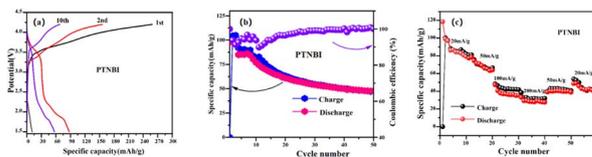

Fig. 6 Charge/discharge curves of PTNBI in SIBs (a), current density: 20 mA g^{-1}. Cycling performance of PTNBI in SIBs (b), current density: 20 mA g^{-1}. Rate capability of PTNBI in SIBs (c).

electrodes over different cycle lengths. As shown in Fig. S7,† the FTIR spectra of the PTNBI electrode before cycling and after 50 cycles show little change, only a decrease in intensity. This indicates that PTNBI was dissolved to a certain extent during cycling. Also, as can be seen from the SEM images (Fig. S8†), the morphology of PTNBI undergoes some changes after 50 cycles. Thus, it can be seen from the above analysis that the structure of the electrode remains basically stable after 50 cycles. In addition, as shown in Fig. S9,† the PTNBI used in LIBs displayed a bigger R_{ct} value than that of the PTNBI used in SIBs before cycling, indicating that the structural stability of the PTNBI used in LIBs was better than that of the PTNBI used in SIBs.

4. Conclusion

In summary, a novel PTNBI electrode has been synthesized through the polymerization of 4-aminotriphenylamine with BTDA, which is used as a cathode material for LIBs/SIBs. The PTNBI exhibits remarkable performance in both LIBs and SIBs. Especially when used as a cathode material for LIBs, the PTNBI electrode delivers a high discharge platform of 3.5 V and a good initial specific discharge capacity of ~135 mA h g^{-1} at 50 mA g^{-1} whilst retaining remarkable cycling stability after 100 cycles. This is attributed to the incorporation of triphenylamine into the organic carbonyl anhydride structure. The formation of polymeric PTNBI effectively reduces the dissolution of TNBI in organic electrolytes. The introduction of triphenylamine effectively improves the discharge platform, and the addition of polycarbonate anhydride effectively enhances its theoretical and practical capacity. The modification of the organic anhydride carbonyl group provides a basis for the modification of other high-capacity organic electrode materials.

Data availability

The data that support the findings of this study are available from the corresponding author upon reasonable request.

Conflicts of interest

There are no conflicts to declare.

Acknowledgements

Fig. 5 CV curves of PTNBI in SIBs (a), scan rate: 0.1 mV s^{-1}. Electrochemical reaction mechanism of PTNBI in SIBs (b).

References

1 D. Zhou, K. Q. Zhang, S. Q. Zou, X. B. Li and H. W. Ma, Conjugated microporous polymers: their synthesis and potential applications in flexible electrodes, *J. Mater. Chem. A*, 2024, **12**, 17021–17053.

2 C. W. Kang, Y. J. Ko, S. M. Lee, H. J. Kim, J. Choi and S. U. Son, Carbon black nanoparticle trapping: a strategy to realize the true energy storage potential of redox-active conjugated microporous polymers, *J. Mater. Chem. A*, 2021, **9**, 17978–17984.

3 L. M. Zhu, G. C. Ding, L. L. Xie, X. Y. Cao, J. P. Liu, X. F. Lei and J. X. Ma, Conjugated carbonyl compounds as high-performance cathode materials for rechargeable batteries, *Chem. Mater.*, 2019, **31**, 8582–8612.

4 H. G. Wang and X. B. Zhang, Organic carbonyl compounds for sodium-ion batteries: recent progress and future perspectives, *Chem.–Eur. J.*, 2018, **24**, 18235–18245.

5 Z. P. Song, H. Zhan and Y. H. Zhou, Polyimides: promising energy-storage materials, *Angew. Chem., Int. Ed.*, 2010, **49**, 8444–8448.

6 H. G. Wang, S. Yuan, D. L. Ma, X. L. Huang, F. L. Meng and X. B. Zhang, Tailored aromatic carbonyl derivative polyimides for high-power and long-cycle sodium-organic batteries, *Adv. Energy Mater.*, 2014, **4**, 1301651.

7 C. Y. Chen, X. Zhao, H. B. Li, F. Gan, J. X. Zhang, J. Dong and Q. H. Zhang, Naphthalene-based polyimide derivatives as organic electrode materials for lithium-ion batteries, *Electrochim. Acta*, 2017, **229**, 387–395.

8 H. Q. Yang, S. W. Liu, L. H. Cao, S. H. Jiang and H. Q. Hou, Superlithiation of non-conductive polyimide toward high performance lithium-ion batteries, *J. Mater. Chem. A*, 2018, **6**, 21216–21224.

9 F. Xu, J. T. Xia and W. Shi, Anthraquinone-based polyimide cathodes for sodium secondary batteries, *Electrochem. Commun.*, 2015, **60**, 117–120.

10 F. Xu, J. T. Xia, W. Shi and S. A. Cao, Electrochemical properties of anthraquinone-based polyimides as cathodes for lithium secondary batteries, *Chem. Lett.*, 2016, **45**, 271–273.

11 F. Xu, H. T. Wang, J. H. Lin, X. Luo, S. A. Cao and H. X. Yang, Poly(anthraquinonyl imide) as a high capacity organic cathode material for Na-ion batteries, *J. Mater. Chem. A*, 2016, **4**, 11491–11497.

12 Z. Q. Luo, L. J. Liu, J. X. Ning, K. X. Lei, Y. Lu, F. J. Li and J. Chen, A microporous covalent-organic framework with abundant accessible carbonyl groups for lithium-ion batteries, *Angew. Chem., Int. Ed.*, 2018, **57**, 9443–9446.

13 M. H. Jung and R. V. Ghorpade, Polyimide containing tricarbonyl moiety as an active cathode for rechargeable Li-ion batteries, *J. Electrochem. Soc.*, 2018, **165**, A2476–A2482.

14 A. V. Mumyatov, A. F. Shestakov, N. N. Dremova, K. J. Stevenson and P. A. Troshin, New naphthalene based polyimide as an environment friendly organic cathode material for lithium batteries, *Energy Technol.*, 2019, **7**, 1801016.

15 S. Lei, X. Cui, X. F. Liu, X. F. Zhang, X. Y. Han and Y. K. Yang, Hydrothermally self-templated synthesis of rectangular polyimide submicrotubes and promising potentials in electrochemical energy storage, *Chem. Commun.*, 2020, **56**, 1429–1432.

16 Z. H. Ba, Z. X. Wang, M. Luo, H. B. Li, T. Huang, J. Dong, Q. H. Zhang and X. Zhao, Benzoquinone-based polyimide derivatives as high capacity and stable organic cathodes for lithium-ion batteries, *ACS Appl. Mater. Interfaces*, 2020, **12**, 807–817.

17 G. Wang, N. Chandrasekhar, B. P. Biswal, D. Becker, S. Paasch, E. Brunner, M. Addicoat, M. H. Yu, R. Berger and X. L. Feng, A crystalline 2D polyarylimide cathode for ultrastable and ultrafast Li storage, *Adv. Mater.*, 2019, **31**, 1901478.

18 J. K. Feng, X. P. Ai, Y. L. Cao and H. X. Yang, Polytriphenylamine used as an electroactive separator material for overcharge protection of rechargeable lithium battery, *J. Power Sources*, 2006, **161**, 545–549.

19 J. K. Feng, Y. L. Cao, X. P. Ai and H. X. Yang, Polytriphenylamine: a high power and high capacity cathode material for rechargeable lithium batteries, *J. Power Sources*, 2008, **177**, 199–204.

20 Z. X. Chen, W. J. Li, Y. Y. Dai, N. Xu, C. Su, J. L. Liu and C. Zhang, Conjugated microporous polymer based on star shaped triphenylamine benzene structure with improved electrochemical performances as the organic cathode material of Li-ion battery, *Electrochim. Acta*, 2018, **286**, 187–194.

21 C. Su, H. H. He, L. H. Xu, K. Zhao, C. C. Zheng and C. Zhang, A mesoporous conjugated polymer based on a high free radical density polytriphenylamine derivative: its preparation and electrochemical performance as a cathode material for Li-ion batteries, *J. Mater. Chem. A*, 2017, **5**, 2701–2709.

22 C. Friebe, B. A. Lex and U. S. Schubert, Sustainable energy storage: recent trends and developments toward fully organic batteries, *ChemSusChem*, 2019, **12**, 4093–4115.

23 L. L. Mo, G. Y. Zhou, P. Ge, Y. E. Miao and T. X. Liu, Flexible polytriphenylamine-based cathodes with reinforced energy storage capacity for high-performance sodium-ion batteries, *Sci. China Mater.*, 2022, **65**, 32–42.

24 Y. P. Li and B. Wang, High rate and ultralong cyclelife fiber-shaped sodium dual-ion battery based on bismuth anodes and polytriphenylamine cathodes, *Battery Energy*, 2023, **2**, 20220035.

25 I. Kang, T. Lee, Y. R. Yoon, J. W. Kim, B. K. Kim, J. Lee, J. H. Lee and S. Y. Kim, Synthesis of arylene ether-type hyperbranched poly(triphenylamine) for lithium battery cathodes, *Materials*, 2021, **14**, 7885.

26 K. Yamamoto, D. Suemasa, K. Masuda, K. Aita and T. Endo, Hyperbranched triphenylamine polymer for ultrafast battery cathode, *ACS Appl. Mater. Interfaces*, 2018, **10**, 6346–6353.

27 Z. P. Song and H. S. Zhou, Towards sustainable and versatile energy storage devices: an overview of organic electrode materials, *Energy Environ. Sci.*, 2013, **6**, 2280–2301.

28 S. Chen, T. Jia, G. Y. Zhou, C. J. Zhang, Q. Hou, Y. H. Wang, S. L. Luo, G. Shi and R. H. Zeng, A Cross linked triphenylamine based polymer cathode material with dual anion cation reversible insertion for lithium-ion battery, *J. Electrochem. Soc.*, 2019, **166**, A2543–A2548.

29 C. Su, B. Han, J. P. Ma and L. H. Xu, A novel anthraquinone-containing poly(triphenylamine) derivative: preparation and electrochemical performance as cathode for lithium-ion batteries, *ChemElectroChem*, 2020, **7**, 4101–4107.

30 K. Li, Y. N. Wang, B. Gao, X. L. Lv, Z. J. Si and H. G. Wang, Conjugated microporous polyarylimides immobilization on carbon nanotubes with improved utilization of carbonyls as cathode materials for lithium/sodium-ion batteries, *J. Colloid Interface Sci.*, 2021, **601**, 446–453.

31 W. R. Huang, T. Jia, G. Y. Zhou, S. Chen, Q. Hou, Y. H. Wang, S. L. Luo, G. Shi and B. J. Xu, A triphenylamine-based polymer with anthraquinone side chain as cathode material in lithium ion batteries, *Electrochim. Acta*, 2018, **283**, 1284–1290.

32 L. H. Xu, G. Z. Wang, S. T. Liu and C. Su, Diphenylamine active unit contained polytriphenylamine derivative and its preparation and electrochemical properties as organic cathode of lithium-ion batteries, *Chem. Eng. J.*, 2025, **509**, 161226.

33 T. Y. Liu, K. C. Kim, B. Lee, S. Jin, M. J. Lee, M. Li, S. Noda, S. S. Jang and S. W. Lee, Enhanced lithium storage of an organic cathode *via* the bipolar mechanism, *ACS Appl. Energy Mater.*, 2020, **3**, 3728–3735.

34 A. N. Zhou, Z. Li, D. Li, C. N. Cheng, X. Chen, Q. F. Wang, A. A. Kasera, J. H. Li, Q. Hou and R. H. Zeng, Triphenylamine-supported benzoquinone polymer as high performance cathode for lithium-ion battery, *ChemistrySelect*, 2024, **9**, e202400538.

35 Y. Wang, N. F. Jia, S. L. Qi, G. F. Tian and D. Z. Wu, Synthesis, characterization and memory performance of naphthalimides containing various electron-withdrawing moieties, *Acta Phys.-Chim. Sin.*, 2017, **33**, 2227–2236.